nature communications

Article

https://doi.org/10.1038/s41467-025-61594-4

Spatially dependent *f*-π exchange interaction within a single-molecule magnet $TbPc_2$

Received: 8 January 2025

Accepted: 25 June 2025

Published online: 07 July 2025

Check for updates

Xin Liao[1,9], Yun Chen[2,9], Tao Xie[1], Rui-Jing Sun[1], Lian-Zhi Yang[1], Chao-Fei Liu[1], Rui Wang[2,3,4], Svetlana Klyatskaya[5], Mario Ruben[5,6,7], Wenhao Zhang[1,8] ✉ & Ying-Shuang Fu[1,8] ✉

Electrically probing the spin state of localized *f* electrons in a rare-earth-based single-molecule magnet, along with understanding its intramolecular magnetic coupling, is of crucial importance for applications in quantum information and advanced spintronics, yet it remains experimentally challenging. Herein, within a single-molecule magnet terbium(III) bis(phthalocyaninato) ($TbPc_2$) double-decker molecule adsorbed on a bilayer graphene epitaxially grown on a SiC(0001) substrate, we experimentally demonstrate a spatially dependent exchange interaction between the magnetic moment of the localized Tb 4*f* electron and the unpaired spin of the Pc π-radical. The magnetic state of $TbPc_2$, associated with the *f*-π interaction, is evidently detected through the spectroscopic Kondo resonance and a zero-field Kondo splitting, which can be reversibly switched in a charge/discharge process triggered by the tip-molecule distance. Furthermore, we theoretically describe how the Kondo resonance evolves at the molecular scale, which is mediated by the *f*-π exchange interaction with its strength varying spatially in a radial decay fashion. Our spatially resolved Kondo characteristics offer a quantitative understanding of the many-body spin correlation, which is coupled with the charge states in a nonuniform and spatially extended system.

Lanthanide-based single-molecule magnets (SMMs) have emerged as key building blocks for developing molecular spintronics and quantum information processing[1–7]. These SMMs exhibit superior magnetic properties and promising performance metrics, including robust magnetic stability, quantum tunneling of magnetization and prolonged spin relaxation dynamics[8–13]. The hybrid architecture—featuring a combination of the lanthanide (Ln) ion encapsulated within delocalized π-electron systems of phthalocyanine (Pc) ligands—boosts the sensitivity of its quantum nature of molecular spin to the local environment. While much attention has been focused on the Pc ligand spin, challenges persist in addressing the large magnetic moment of the Ln ion in SMMs. This difficulty arises from the highly localized nature of the 4*f*-shell orbitals of Ln ions, which have minimal participation in electron tunneling currents through the molecule[14–17].

The *f*-π interaction has been actively investigated by single-molecule transistor experiments. The derived interaction is however controversial with both ferromagnetic[1,17,18] and antiferromagnetic[19,20] interactions reported. More importantly, these macroscopic transport

[1]School of Physics and Wuhan National High Magnetic Field Center, Huazhong University of Science and Technology, Wuhan, China. [2]National Laboratory of Solid State Microstructures and Department of Physics, Nanjing University, Nanjing, China. [3]Collaborative Innovation Center of Advanced Microstructures, Nanjing University, Nanjing, China. [4]Jiangsu Physical Science Research Center, Nanjing, China. [5]Institute of Nanotechnology, Karlsruhe Institute of Technology, Eggenstein-Leopoldshafen, Germany. [6]Institute for Quantum Materials and Technologies, Karlsruhe Institute of Technology, Eggenstein-Leopoldshafen, Germany. [7]Centre Européen de Sciences Quantiques, Institut de Science et d'Ingénierie Supramoléculaires, Strasbourg Cedex, France. [8]Wuhan Institute of Quantum Technology, Wuhan, China. [9]These authors contributed equally: Xin Liao, Yun Chen. ✉e-mail: wenhaozhang@hust.edu.cn; yfu@hust.edu.cn

measurements lack the ability to reveal the spatial information of the exchange interaction within the SMMs. Recent advances in scanning tunneling microscopy and spectroscopy (STM/STS) studies have explored the localized *f* states in Ln-based SMMs through the Kondo effect, a many-body phenomenon that occurs when a localized magnetic moment interacts with the conduction electrons of a host metal. Representative studies include spectroscopic characterizations of the Kondo effect from the *f*-orbitals that are either directly spin-screened by the conduction electrons in $NdPc_2$[21], or facilitated by the strong hybridization between the ligands and metal substrates in $DyPc_2$[22]. However, as the Ln ion presents a highly anisotropic large magnetic moment, the mechanism underlying how the spin-flip scattering takes place remains largely mysterious. Alternatively, an indirect readout of the 4*f* spin via a split Kondo resonance of the ligand spin is implemented, as induced by the *f*-π coupling[23]. Yet, the Kondo effect therein can be only observed on the Pc lobes, and is completely suppressed on the Ln ion. This precludes the detection of the Ln-radical exchange interactions, which are expected to happen dominantly around the Ln ion[15,24–27]. Fundamentally, it is also of significant importance to clarify the Kondo behavior in the presence of exchange interaction between a highly localized *f*-moment and an extended π-radical orbital.

In this study, we utilize high-spatial and high-energy resolution STM/STS to investigate the spin state of the $TbPc_2$ molecule adsorbed onto a graphene-covered SiC substrate. Through adjusting the STM tip height, the $TbPc_2$ molecule is reversibly switched between neutral and charged ground states, switching on/off the Kondo resonance. In the neutral state of $TbPc_2$, its Kondo peak around the Tb^{3+} ion shows a sizable zero-field splitting of 1.14 meV, which decays spatially away from the molecular center. The zero-field splitting enlarges under magnetic fields, unambiguously demonstrating a ferromagnetic *f*-π coupling. We develop a generalized Anderson model based on a proposed density Hamiltonian to describe the exchange coupling between the localized *f* moment and the extended π spin, which reproduces the experimental findings. The tunability of the discharging-driven Kondo effect, combined with the spatial resolution of the Ln-radical exchange interactions, holds the potential to search for intricate details of Kondo physics.

Results and discussion

Tip-tuned Kondo effect of $TbPc_2$ molecule

An isolated $TbPc_2$ molecule consists of a Tb^{3+} ion at the center, and two sandwiched Pc ligands that are stacked with a mutual rotation of 45° relative to each other (Fig. 1a). In its neutral state, the central Tb^{3+} ion hosts a highly localized 4*f*-electron moment. Meanwhile, the two Pc ligands bear one unpaired electron with spin $S = 1/2$, which is delocalized over the π-radical orbital[9,15]. When adsorbed onto graphene substrates, $TbPc_2$ molecules form a square checkerboard film with the molecular height of ≈0.7 nm, consistent with the intact double-decker structure (Supplementary Fig. 1). The STM image of $TbPc_2$ in Fig. 1b features an eight-lobed structure, which conforms to the density of states (DOS) of the highest occupied and lowest unoccupied molecular orbitals (HOMO and LUMO) of the upper Pc ligand[14,15]. Tunneling spectra of the $TbPc_2$ molecule in Fig. 1c indicate its HOMO and LUMO are located at −1.0 eV and +0.7 eV, respectively. There is a clear energy shift of the molecular orbitals between the Tb center and the lobe site. A similar shift has also been observed in $NdPc_2$ and $DyPc_2$, and was attributed to an electrostatic field effect[21,22]. However, there are also notable differences when compared to $NdPc_2$ and $DyPc_2$. Specifically, the LUMO state of $TbPc_2$ is ≈0.3 eV closer to the Fermi level (E_F).

As depicted in Fig. 1d, the low-energy spectrum of the molecule, obtained at a set current (I_t) of 0.1 nA, is featureless around E_F. This implies the ligand spin is absent, as being paired up by an additional electron transferred from the substrate[27,28]. Surprisingly, upon acquiring spectrum with a large I_t of 0.5 nA, a sharp Kondo peak emerges around E_F, which stays unchanged with even larger I_t but disappears again upon reducing I_t to 0.1 nA (Fig. 1d). This observation demonstrates that the ligand spin state reversibly switches with I_t, as caused by the charging and discharging of the ligand orbital. To track

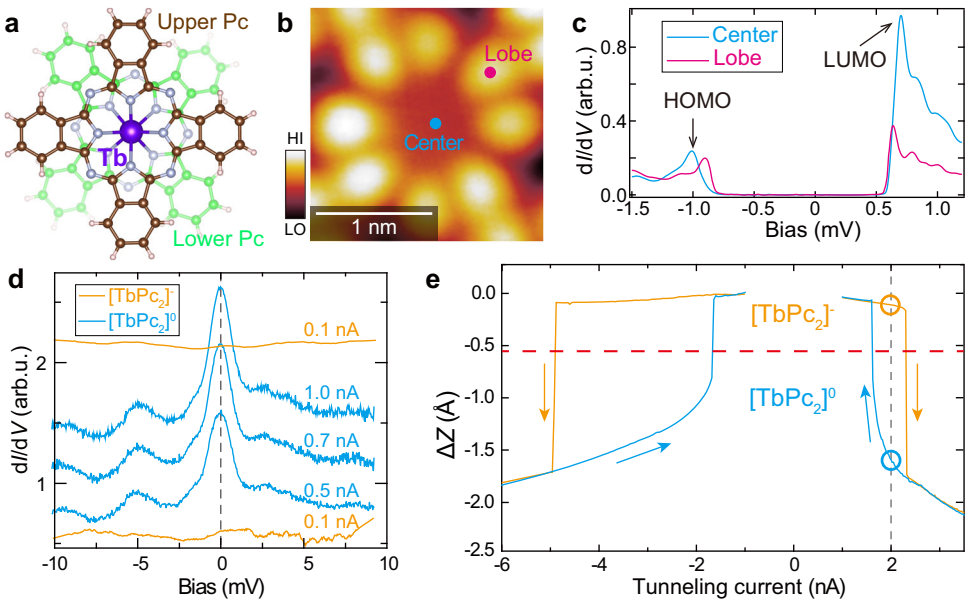

Fig. 1 | The emerging Kondo resonance of $TbPc_2$ on graphene. a Schematic illustration for $TbPc_2$ molecule in a top view, showing the central Tb atom surrounded by the upper (dark brown) and lower (light green) Pc ligands with a 45° rotation. **b** Corresponding high-resolution STM image of a single $TbPc_2$ molecule obtained at occupied states ($V_b = -1.0$ V and $I_t = 10$ pA, 2×2 nm^2). **c** Large-scale d*I*/d*V* spectra taken at the Tb center (cyan) and Pc lobe (magenta) site, respectively ($V_b = -1.5$ V and $I_t = 100$ pA, $V_{mod} = 20$ mV). **d** d*I*/d*V* spectra taken at the lobe of the top Pc ligand, which are acquired with various tunneling currents, respectively. Set points: $V_b = 10$ mV and $V_{mod} = 0.1$ mV. **e** Δ*Z*-*I* curves acquired at the lobe site with a constant bias of +10 (−6) mV for the positive (negative) cycle. The scanning sequences in the forward (orange) and backward (cyan) directions are indicated by arrows. At $I_t = 2$ nA, the existence of Kondo resonance is dependent on the history of voltage ramping. For the $[TbPc_2]^0$ ($[TbPc_2]^-$) state with cyan (orange) circle, the corresponding STS spectrum is the same as the cyan (orange) curves in **d**. Regions for different charged states are separated by red dash line. Source data are provided as a Source Data file.

https://doi.org/10.1038/s41467-025-61594-4

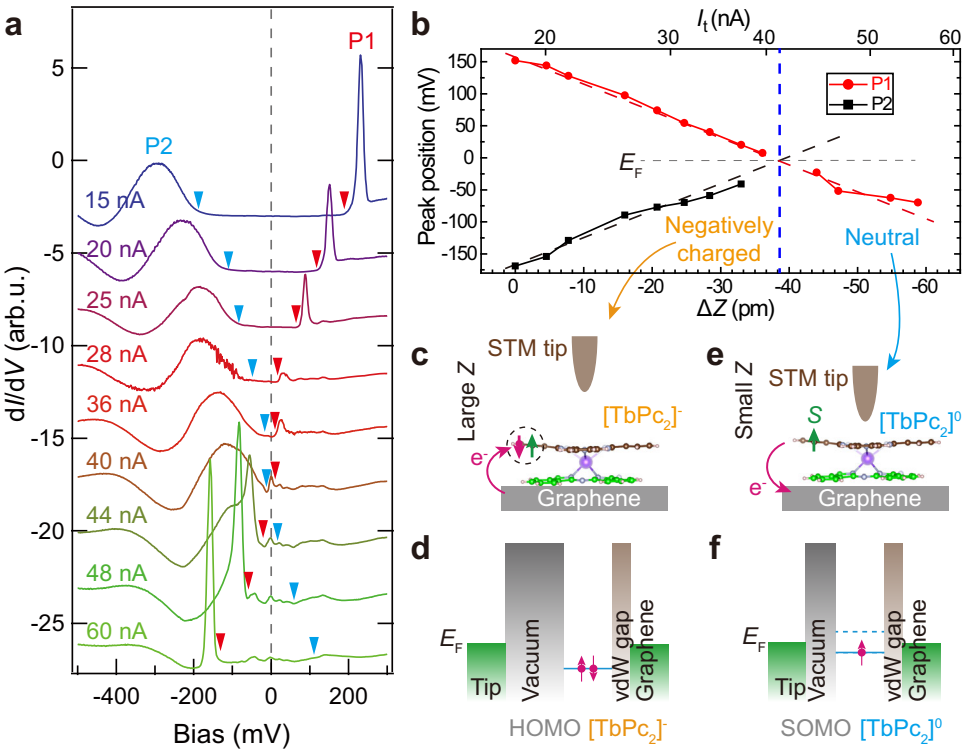

Fig. 2 | Transition of the charging state by a STM tip. a Series of large-energy STS spectra recorded at the same location but with increasing tunneling current (V_b = −0.5 V and V_{mod} = 5 mV). Spectra are offset vertically for clarity. Two featured peaks are labeled as P1 and P2, respectively, with their onsets marked by red and cyan triangles. **b** Evolutions of peak onsets as a function of the tip-sample distance for P1 (red) and P2 (black). Dashed lines are the linear guide for an eye. Vertical dashed blue line highlights the different charged states of the $TbPc_2$ molecule, which are distinguished when P1 crosses E_F. **c, e** Schematic depictions of the molecular spin before (**c**, $[TbPc_2]^-$) and after (**e**, $[TbPc_2]^0$) the tip-triggered discharging transition. **d, f** Potential energy diagrams for the tunneling process through the molecular level of $TbPc_2$, which is paired up to become HOMO by the substrate-induced charge transfer at equilibrium (V_b = 0) for $[TbPc_2]^-$. Conversely, the $[TbPc_2]^0$ restores the SOMO with an unpaired radical spin, showing the Kondo resonance. Source data are provided as a Source Data file.

the charge state transition process, we record the tip-height displacements (ΔZ) by continuously ramping I_t over a wide range, while keeping a constant bias voltage. As shown in Fig. 1e, the $\Delta Z(I)$ curves exhibit obvious hysteresis characteristics for both positive and negative set biases with abrupt jumps in ΔZ, signifying the charge state transition with an electron on/off the $TbPc_2$ molecule[29,30]. While the $TbPc_2$ film is arranged in a checkerboard lattice on graphene, we observe that the emergence of Kondo resonance is irrelevant to the molecular orientation with respect to the graphene substrate, indicative of a negligible influence of molecule-substrate interaction (more discussions can be seen in Supplementary Note 1 and Supplementary Figs. 1–3). Moreover, this phenomenon remains robust against variations of the local environment with different neighboring $TbPc_2$ molecules, suggesting that the molecule-molecule interaction should not dictate the observed Kondo signature.

To unveil the charging mechanism, we further examine the evolution of molecular states with varying I_t. As seen in Fig. 2a, b sharp peak P1 and a broad peak P2 are observed at positive and negative biases, respectively. With decreasing tip height Z, P1 and P2 both gradually shift towards until crossing E_F, and then move away from E_F. The onset energies of P1 and P2 both follow a linear relationship with Z (Fig. 2b), which is reminiscent of resonant tunneling through the same molecular orbital in a double barrier tunneling junction (DBTJ)[31–33]. The two tunnel barriers, with one being the tip-molecule vacuum and the other being the molecule-graphene van der Waals gap, experience a two-step tunneling process with different relative tunneling rates for various ΔZ. Due to the voltage division effect of DBTJ, the two-step tunneling is controlled by a critical parameter of lever arm α, which denotes the fraction of voltage $TbPc_2$ suffers[34–36]. For the narrow-energy measurements with indispensable α, such a voltage drop (αV_b) across the molecule-substrate junction shifts the HOMO level of the $TbPc_2$ molecule. Once the HOMO level is aligned with the chemical potential of the substrate (positive bias) or the tip (negative bias), resonant tunneling occurs between graphene and $TbPc_2$ (P1 for $V_b > 0$) or between the tip and $TbPc_2$ (P2 for $V_b < 0$). In this context, the emergences of P1 and P2 features are due to tunneling through the same HOMO of the $TbPc_2$ molecule at opposite bias polarities, with their energy positions corresponding to the voltage threshold for energy alignment. Within the DBTJ model[31–33], by analyzing the relative energy positions of the P1 and P2 peaks in Fig. 2b, we can estimate the level arm parameter α to be in the range of 0.48-0.67. This relatively large value of α (exceeding 0.5) for a decreased Z is favorable for locally gating the molecular level and provoking its discharge.

Initially, the $TbPc_2$ molecule gains an additional electron from the substrate to become negatively charged $[TbPc_2]^-$, whose otherwise singly occupied molecular orbital (SOMO) becomes a doubly occupied HOMO and thus nonmagnetic (Fig. 2c, d). With decreasing Z, the increased α leads to a smaller threshold required for resonant tunneling, resulting in the reversal shift of P1 and P2 in energy, which is discussed in Supplementary Note 2 and Supplementary Fig. 4. Once the threshold energy is shifted below E_F (cyan region in Fig. 2b), the transferred charge escapes back to the substrate (Fig. 2e). Consequently, the molecule discharges to restore the neutral molecule $[TbPc_2]^0$ with unpaired radical spin, as shown in Fig. 2f. This discharging process induces the transformation of the HOMO into the SOMO with unpaired ligand spin, contributing to the emergence of the spin 1/2 Kondo effect in Fig. 1d. Notably, although the structural configuration of the $TbPc_2$ molecule may be influenced during surface

https://doi.org/10.1038/s41467-025-61594-4

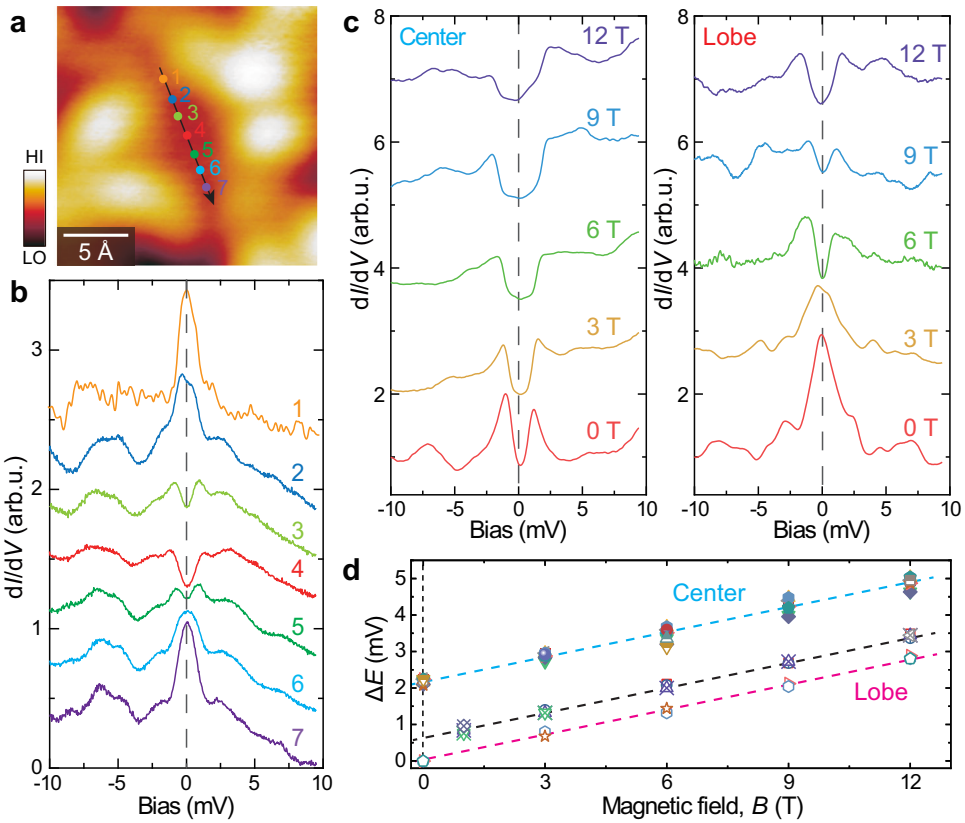

Fig. 3 | Spatially varied Kondo resonance in $TbPc_2$. **a** STM image of $TbPc_2$ obtained at unoccupied states (V_b = +0.8 V and I_t = 10 pA, 2 × 2 nm^2). **b** Comparison of STS spectra taken at the 1–7 locations across the $TbPc_2$ molecule labeled in (**a**) (V_b = 10 mV and I_t = 0.5 nA, V_{mod} = 0.1 mV). The vertical dashed black lines highlight E_F. **c** Magnetic field dependence of the splitting of Kondo resonance taken at the lobe and center, respectively. **d** Splitting energy (ΔE) as a function of the magnetic field. The dashed lines are the linear fittings for the lobe (cyan) and center (purple) positions, respectively. The black series is acquired at a location slightly away from the lobe site. Different colored symbols represent different molecules. Source data are provided as a Source Data file.

deposition and discharge processes, any resulting variations are minimal and do not significantly affect the observed Kondo signatures, as discussed in Supplementary Note 3 and Supplementary Fig. 5. Our tip-driven transition between the neutral and charged states, accompanied by the on/off Kondo state, offers a controllable means of accessing and manipulating the molecular spin in a stable and reversible manner, rather than a temporary charged state, as revealed previously in TCNQ[34], TBTAP[35], $LuPc_2$[36], and DCA molecules[37].

Zero-field Kondo splitting and Zeeman effect

Having identified the Kondo effect of the radical spin for the Pc lobe, we now turn to scrutinize the 4*f*-electron spin at the Tb center. As illustrated in Fig. 3a, b, an elaborate distribution of STS at I_t = 0.5 nA shows the spatial dependence of the Kondo effect along the black arrow in the interior of a $TbPc_2$ molecule. Obviously, the pronounced Kondo resonance is symmetric among different lobes and shows the most significant peak at the Pc ligands. Upon approaching the center of the molecule (Tb^{3+} ion), the Kondo peak gradually gets suppressed and further shows a conductance dip at E_F with symmetric peaks at ±1.14 meV. At the bridge site between the lobe and the center, there exists a prominent hump along with a progressively smaller dip, suggesting it is in the transitional state. In short, the Kondo peak at the Pc ligand gradually splits into a gap-like spin excitation when approaching the Tb^{3+} ion, and has the largest splitting energy at the Tb center. Accordingly, there exists a plain anti-correlated relationship between the peak intensity and splitting gap (Supplementary Figs. 6 and 7).

Interestingly, the Kondo splitting at the Tb^{3+} ion can be observed only when the ligand spin is unpaired. Otherwise, its STS appears featureless and resembles what is observed at the lobe site (Supplementary Fig. 8). This implies that the magnetic state of the $TbPc_2$ molecule should be strongly influenced by the concurrent interaction between the unpaired electron and the Tb 4*f*-electron moment. To confirm this hypothesis, a systematic measurement of a series of dI/dV curves is performed by gradually increasing I_t at different locations. We find that the splitting gap increases in a monotonic manner with decreasing lateral distance to the Tb center. Meanwhile, it keeps constant regardless of the variation in tip heights at each fixed location (as depicted in Supplementary Fig. 9). This suggests the presence of a direct exchange interaction of ferromagnetic coupling between the ligand 1/2 spin and the Tb 4*f* moment. Our maximum splitting energy at the Tb center (≈1.14 meV) is comparable to the reported upper limit of exchange interaction (≈1.3 meV) between a spin-1/2 Ti atom and a static Fe moment[38]. Additionally, previous calculations have reported an energy difference of ≈1.0 meV between the ferromagnetic ($|\pm 6, \pm 1/2\rangle$) and antiferromagnetic ($|\pm 6, \mp 1/2\rangle$) coupling states of the Tb 4*f* and ligand spins in $TbPc_2$[39–41], which reasonably aligns with our experimental value. In this light, the magnetic moment of the localized 4*f* electron is indeed detectable via the Kondo splitting, which should predominantly rely on the intramolecular interaction.

To advocate the spin character of the $TbPc_2$ molecule, we further apply an external magnetic field up to 12 T, which is oriented normal to the surface plane. Figure 3c depicts the magnetic field dependence of the Kondo splitting acquired at the lobe and center sites, respectively. Apparently, the Kondo peak at the Pc ligand becomes split with the largest energy separation under 12 T, indicating that the energies of the two degenerate spin states are lifted. Additionally, the spin excitation of Kondo splitting at the Tb center is progressively increased, which

can be attributed to the Zeeman coupling with out-of-plane spin components, also well excluding any possible origin related to vibrations. By further extracting the splitting energy (ΔE) as a function of the magnetic field in Fig. 3d, both the center and lobe sites follow a linear evolution. These are well consistent with the $\Delta E = 2g\mu_B B$ relation[29,42], where g is the Landé factor and $\mu_B = e\hbar/(2m_0)$ is the Bohr magneton with m_0 being the mass of the electron. By fitting, we obtain the same Landé g-factor as ≈2.0 for both the Tb and radical. Notably, the residual energy separation at zero field (or magnetic remanence) is calculated as 2.2 meV, consistent with Fig. 3b. Such a finite intersection is analogous to the nonvanishing intercept of resonance frequency at $B = 0$ T by ESR-STM experiments[43], signaling that the zero-field splitting should be attributed to the intramolecular exchange interaction between the Pc ligand π-orbital and the Tb 4f electron, and intrinsically contributing net magnetization. It should be noted that the fitting $g = 2$ is expected for the $S = 1/2$ π-radical, which is in good agreement with previous reports on $TbPc_2$ and $DyPc_2$[1,23]. However, the obtained g factor of 2 for the Tb^{3+} ion significantly deviates from its expected value of 3/2[9,39]. The uniform $g = 2$ throughout the $TbPc_2$ molecule in Fig. 3d suggests that the 1/2 spin of the π-radical should take part in the Kondo screening for the entire $TbPc_2$ molecule, including the exchange interaction with the total angular momentum ($J = 6$) of the Tb ion. Furthermore, the Kondo splitting exhibits an identical dependence on the out-of-plane magnetic field in opposite directions, in line with the two-fold degenerate states of $|\pm 6, \mp\frac{1}{2}>$ and $|\pm 6, \pm\frac{1}{2}>$ at zero magnetic field, as discussed in Supplementary Note 4 and Supplementary Fig. 10.

For comparison, we have also deposited and measured YPc_2 molecules on the same substrate, where YPc_2 has an unpaired ligand electron, but its Y^{3+} ion has no 4f electron[27]. As displayed in Supplementary Fig. 11, the YPc_2 molecule shows similar molecular orbitals and gap size as those of $TbPc_2$ in Fig. 1. Moreover, the emergence of Kondo resonance at the Pc lobe is identical to that in $TbPc_2$, which is reproducibly controlled by the discharging process of a charged-to-neutral transition driven by the STM tip height. However, the spatial distribution from the STS linecut within the YPc_2 molecule indicates that there is no splitting of the Kondo peak both on the molecular center and the lobe (Supplementary Fig. 12). Instead, the Kondo shape remains unchanged throughout the whole YPc_2 molecule, which is in line with the extension of the π-radical spin over the two Pc-ligands. The magnetic field dependence of the Kondo splitting for the YPc_2 also yields a g-factor of ≈2.0. All these observations collectively signal that the 4f electron moment and its exchange coupling to the unpaired radical spin play a crucial role in the Kondo splitting for the ground state of the Ln-based SMMs.

Theoretical model for the spatially resolved Kondo effect

Theoretically, we model the $TbPc_2$ on the graphene substrate by a generalized Anderson-type model. Using the numerical renormalization group (NRG) method, we reveal a Kondo effect mediated by the intramolecular exchange interaction, which explains the spatially dependent Kondo resonance in Fig. 3b. The spatially extended π-radical orbital of the Pc ligands, denoted by $u_\sigma(\mathbf{r})$, is coupled to the 4f electrons of the central Tb^{3+} ion, via $H_c = \sum_\sigma \int d\mathbf{r} t(\mathbf{r}-\mathbf{r}_0) u^\dagger_{\mathbf{r},\sigma} v_{\mathbf{r}_0,\sigma} + \text{h.c.}$, where $u_{\mathbf{r},\sigma}$ and $v_{\mathbf{r}_0,\sigma}$ are the second-quantized operators for the Pc and Tb electrons at coordinate $\mathbf{r}$, respectively. Here, "h.c." corresponds to the Hermitian conjugate of the preceding term. The coupling $t(\mathbf{r}-\mathbf{r}_0)$ decays with the distance $|\mathbf{r}-\mathbf{r}_0|$, where $\mathbf{r}$ stands for the spatial coordinate within the $TbPc_2$ molecule, $\mathbf{r}_0$ denotes the location of the Tb^{3+} ion, which is taken as the origin ($\mathbf{r}_0 = 0$) in what follows. The Pc electrons are captured by $H_{Pc} = \varepsilon_0 \sum_\sigma \int d\mathbf{r} u^\dagger_{\mathbf{r},\sigma} u_{\mathbf{r},\sigma} + \frac{U}{2}\sum_\sigma \int d\mathbf{r} d\mathbf{r}' u^\dagger_{\mathbf{r},\sigma} u_{\mathbf{r},\sigma} u^\dagger_{\mathbf{r}',\bar{\sigma}} u_{\mathbf{r}',\bar{\sigma}}$, where ε_0 is the orbital energy and U is the repulsive electron-electron interaction. As schematically shown in Fig. 4a, the Pc electrons are further coupled to the graphene substrate (conduction bath) as that of the standard Anderson model, which is not written explicitly.

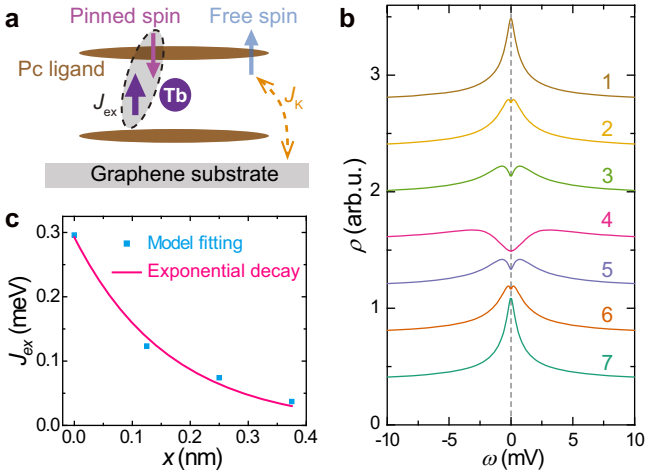

Fig. 4 | Kondo evolution calculated by NRG. a Schematic plot of the Kondo mechanism. The spin density operator of the Pc π-orbital has a spatially dependent property. Around the center, it is strongly pinned by the local moment of the Tb^{3+} ion. However, it behaves approximately as a free spin at the lobe far from the center. The Kondo resonance thus occurs for larger r after J_K is further considered, which splits for small r. **b** Calculated local density of states with varying J_{ex} (or r). From top to bottom, $J_{ex} = 0.04$, 0.07, 0.12, 0.30, 0.12, 0.07, 0.04 meV, corresponding to the process when the STM probe is moved from one edge of the ligand to the center and further to the other edge. Both inelastic and elastic scattering processes have been considered, whose ratio is set to be $k = 0.05$. The parameters used are $D = -40$ meV, $N_0 J_K = 60$ meV with N_0 being the bath density of states at the Fermi energy. The states kept are 1024 in the NRG calculations with the scaling parameter $\Lambda = 2.5$. **c** Extracted r-dependence of the exchange coupling J_{ex}, which is well fit by an exponential function $J_{ex} = J_0 e^{-r/\xi}$ with $J_0 = 0.29$ meV, and $\xi = 0.16$nm. Source data are provided as a Source Data file.

We perform the Schrieffer-Wolff transformation by tracing out the doubly occupied state of Pc electrons, which leads to the Kondo exchange type interaction, $H_J = \int d\mathbf{r} h_J(\mathbf{r})$, where

$$h_J = \frac{1}{2} J_K \sum_{\mathbf{k},\mathbf{k}',\sigma,\sigma'} \mathbf{S}_{Pc} \cdot c^\dagger_{\mathbf{k},\sigma} \boldsymbol{\sigma}_{\sigma\sigma'} c_{\mathbf{k},\sigma'} + J_{ex}(\mathbf{r}) \mathbf{S}_{Tb} \cdot \mathbf{S}_{Pc} \quad (1)$$

The first term describes the Kondo coupling between the Pc electrons and the graphene substrate, with J_K the coupling strength. $\mathbf{S}_{Pc} = \frac{1}{2} u^\dagger_\sigma \boldsymbol{\sigma}_{\sigma\sigma'} u_{\sigma'}$ is the spin-1/2 operator contributed by the Pc electron, where $u_\sigma = \frac{1}{A}\int d\mathbf{r} u_{\mathbf{r},\sigma}$ is the coarse-grained fermionic field with A being the area of the π-orbital. The second term is the exchange coupling between the Tb^{3+} ion and the radical spin of the Pc ligand, which has spatial dependence, with $J_{ex}(\mathbf{r}) \propto |t(\mathbf{r})|^2/U$. $\mathbf{S}_{Tb}$ is the effective spin operator of the Tb ion, and $S_{Tb} = 6$ is taken with a magnetic anisotropy term of $H_{ani} = DS^2_{Tb,z}$. We emphasize that although the experimental system is described by the full Hamiltonian $H_J = \int d\mathbf{r} h_J(\mathbf{r})$, it is however the density Hamiltonian $h_J(\mathbf{r})$ in Eq.(1) that is relevant to the STM/STS measurements. The spatial dependence in $h_J(\mathbf{r})$ has non-negligible physical consequences, but is largely neglected in previous theoretical studies.

Further considering the graphene thermal bath, the local Hamiltonian (at $\mathbf{r}$) relevant to STM/STS measurements is obtained as $h_J + H_{ani} + H_{bath}$. We map this model to the half-infinite Wilson chain in the NRG framework, where the first chain site (describing the Tb ion) interacts with the second site (representing the Pc spin) via $J_{ex}(\mathbf{r})$. We then solve the chain model and calculate the local spectral density at generic $\mathbf{r}$, considering both the elastic and inelastic tunneling processes (see Supplementary Notes 5 and 6). As shown by Fig. 4b, when the STM tip is moving from the lobe towards the central Tb ion, $J_{ex}(\mathbf{r})$ increases, and the spectra gradually evolve from a Kondo peak to a significant dip. This indicates a spatially varying property of the spin

density operator of the Pc π-orbital. Before the Kondo effect sets in, $\mathbf{S}_{Pc}$ behaves as a free spin at the lobe far away from the center, but is strongly pinned by the Tb ion around the center (Fig. 4a). Thus, the Kondo screening can easily take place for large $r = |\mathbf{r}|$, but is suppressed around the center due to the strong exchange field from the Tb ion, resulting in the splitting feature for small r. The numerical results well reproduce the spatially varied Kondo resonance in our STM observations. Furthermore, by fitting to the experimentally measured height (depth) of the peak (dip) from the STS spectra in Fig. 3b, the $\mathbf{r}$-dependence of $J_{ex}(\mathbf{r})$ can be numerically extracted as shown in Fig. 4c, which shows an exponential decay[38,44]. All these results reveal a Kondo effect mediated by the intramolecular exchange interaction, i.e., a spatially varying Kondo phenomena distributed in extended molecule orbitals.

Discussion

We exclude several alternative explanations for the observed phenomena. Firstly, the direct substrate exchange is unlikely, as the graphene substrate lacks magnetic moments, and such interaction would preferentially favor stronger influences for the closer Pc ligand, contrary to the observed splitting localized at the distant Tb^{3+} site. Secondly, control experiments using YPc_2 (identical ligand structure and π spin system in Supplementary Figs. 11 and 12) exhibit homogeneous Kondo resonance without zero-field splitting, thereby ruling out both ligand-mediated intermolecular interactions and ligand-field effects as the primary origin of the splitting in $TbPc_2$. In addition, the insensitivity to the local environment reinforces the exclusion of intermolecular effects. Furthermore, spin-orbit coupling (SOC) should not be the driving mechanism, since Kramers theorem dictates the ground state remains degenerate at zero field for the $S = 1/2$ ligand spin, preventing SOC-induced Kondo splitting. Previous studies on $TbPc_2$ and related $LnPc_2$ molecules[14,15,21,22,27], even those with stronger SOC, confirm the absence of such splitting. Ultimately, the pronounced spatial dependence provides compelling evidence against purely isotropic or molecule-wide mechanisms like ligand-field or SOC effects acting alone. Instead, it strongly supports our interpretation of the splitting arising from a spatially distributed intramolecular f-π exchange interaction between the Tb^{3+} 4f electrons and the ligand π-radical spin.

Finally, we elucidate the influence of the graphene-covered SiC substrate, which is instrumental to our observation of the intramolecular f-π exchange coupling within $TbPc_2$. Unlike metallic substrates where strong molecule-substrate hybridization typically yields a broad Kondo resonance width (5–9 meV)[22,27], masking fine spectral details, graphene provides significant electronic decoupling. This preserves the intrinsic molecular properties while still permitting charge-state control, a feature often hindered on insulating layers[43]. Crucially, the low carrier density of graphene/SiC results in a narrow Kondo width (≈1 meV), enabling the resolution of the subtle splitting energy scale caused by the f-π exchange coupling (1.1 meV). In this light, graphene uniquely preserves the $TbPc_2$ molecule's intrinsic spin characteristics with the possibility of controlled charge transfer. This highlights $TbPc_2$/graphene as a promising platform for the electronic control of SMMs in molecular spintronics. For instance, the distinct Kondo switching ("on/off") allows a direct manipulation of spin-state transition and magnetic toggling with electronic precision in SMM-based transistors. Moreover, the spatial dependence of the f-π exchange interaction acts as an electrically readable signature for probing localized 4f moments at a single-molecule level. Leveraging the graphene substrate, external gate voltages could be employed to tune the concentration of conduction electrons. This offers a pathway towards a gate-tunable Kondo resonance for precisely interrogating and continuously controlling the magnetic properties of SMMs in device architectures.

As a summary, we investigate the spin state of the $TbPc_2$ molecule through a tip-induced discharging process at the atomic level. The 4f moment of the central Tb^{3+} ion, together with its magnetic exchange coupling to the $S = 1/2$ Pc ligand spin, is evidenced by the Kondo resonance and zero-field splitting. The spatial variation of the Kondo characteristic unambiguously reveals the spatial confinement of the Ln moment, providing an alternative route to electronically access the localized 4f moment with variable coupling to the unpaired ligand electron within an individual SMM. Our theoretical modeling identifies an exchange-interaction-mediated Kondo effect by considering the radial distribution of molecular orbits and f-π exchange coupling strength within the $TbPc_2$ molecule, well explaining the spectroscopic data. Since the split Kondo peaks are expected to be fully spin-polarized[45], the different charged states governed by the local electric gating of the STM tip may shed light on developing promising molecular spin transistors for highly efficient electronic read-out, involving charge transport with current flowing through both the Ln center and Pc ligands.

Methods

$TbPc_2$ and YPc_2 films growth

$TbPc_2$ and YPc_2 were synthesized according to ref. 46 and analytical data confirm their intact structure and high purity. Before growth, a uniform graphene-covered SiC(0001) substrate was first prepared in the ultrahigh-vacuum chamber by the processing method following ref. 47. High-purity $TbPc_2$ molecules were thermally evaporated at ≈400 °C from a homemade Knudsen cell, then onto the preprepared graphene-covered SiC substrate at room temperature. We have obtained mono-, bi-, and tri-layer graphene on the SiC substrate, where the bilayer graphene dominates the surface area. We find that the molecular structure and orientation of the $TbPc_2$ film keep the same on different thicknesses of graphene. Additionally, the characteristic Kondo resonance and splitting features were consistently observed at all the obtained graphene layers.

STM/STS measurements

The STM/STS experiments were carried out with a custom-designed ultrahigh vacuum STM system (Unisoku-1300) at a base temperature of 0.4 K[48]. An electro-etched W wire was used as the STM probe, which had been cleaned and characterized on a Cu(111) crystal prior to the measurements. The dI/dV spectra were acquired using a conventional lock-in technique with a modulation voltage at 983 Hz feeding into the sample bias. To obtain the dI/dV spectrum with an increased I_t, the tip is stabilized in a constant-height mode with the feedback loop off, thus freezing the tip height Z during sweeping the bias voltage. $\Delta Z = 0$ is defined as the initial tip position recorded for the smallest I_t. The ΔZ-I spectroscopy is implemented by incrementally ramping I and simultaneously recording Z, which is dynamically adjusted by the tip position to maintain a given bias setpoint. An external magnetic field up to 12 T is applied perpendicular to the surface plane. All topographic images were taken in a constant-current mode, and were processed using Gwyddion.

Under the conditions necessary for high-resolution STS mapping at a low bias (typically involving close tip-sample proximity and potentially higher tunneling currents for a sufficient signal-to-noise level), the $TbPc_2$ molecule is highly susceptible to tip-induced displacement during the scanning process. When the tip approaches the molecule in a discharging state, the $TbPc_2$ is easily adsorbed onto the tip or dragged laterally upon performing spectroscopic mapping. This disrupts its original position and precludes stable acquisition of spatially continuous STS linecut or dI/dV maps across a single molecule. To mitigate this limitation while ensuring data integrity, after acquiring each STS curve, we immediately capture a follow-up STM image to confirm the molecule's location and structural integrity. This protocol guarantees that all spectroscopic data are collected from undisturbed $TbPc_2$ molecules in their native configuration. Our systematic and reproducible observations, across multiple molecules and

experimental sessions, provide robust evidence for the spatially dependent *f-π* interaction central to our findings.

Theory

Density functional theory (DFT) calculations were executed using the Vienna ab initio simulation package (VASP)[49,50]. The calculations employed the projected augmented wave method[51]. For the exchange-correlation function, we adopted the one proposed by Hamada[52], which incorporates non-local corrections through van der Waals interactions. The VASPKIT package served to analyze the computational data. We used the pseudopotential of the Tb^{3+} ion with a fixed 4*f* electronic state. This approach is a standard practice for evaluating the electronic states of ligands within phthalocyanine molecules[53]. During structural optimization, the force was constrained to be less than 0.02 eV $Å^{-1}$, and the convergence criterion for the total energy was set at 1×10^{-5} eV. To sample the Brillouin zone, we utilized a $1 \times 1 \times 1$ Gamma-centered k-point grid.

Data availability

The data that support the findings of this study are available from Zenodo[54] and from the corresponding authors upon request. Source data are provided with this paper.

Code availability

The code used in this study is available from the corresponding authors upon request.

References

1. Vincent, R., Klyatskaya, S., Ruben, M., Wernsdorfer, W. & Balestro, F. Electronic read-out of a single nuclear spin using a molecular spin transistor. *Nature* **488**, 357–360 (2012).
2. Ganzhorn, M., Klyatskaya, S., Ruben, M. & Wernsdorfer, W. Strong spin–phonon coupling between a single-molecule magnet and a carbon nanotube nanoelectromechanical system. *Nat. Nanotechnol.* **8**, 165–169 (2013).
3. Thiele, S. et al. Electrical readout of individual nuclear spin trajectories in a single-molecule magnet spin transistor. *Phys. Rev. Lett.* **111**, 037203 (2013).
4. Goodwin, C. A., Ortu, F., Reta, D., Chilton, N. F. & Mills, D. P. Molecular magnetic hysteresis at 60 Kelvin in dysprosocenium. *Nature* **548**, 439–442 (2017).
5. Godfrin, C. et al. Operating quantum states in single magnetic molecules: implementation of Grover's quantum algorithm. *Phys. Rev. Lett.* **119**, 187702 (2017).
6. Guo, F.-S. et al. Magnetic hysteresis up to 80 Kelvin in a dysprosium metallocene single-molecule magnet. *Science* **362**, 1400–1403 (2018).
7. Moreno-Pineda, E. & Wernsdorfer, W. Measuring molecular magnets for quantum technologies. *Nat. Rev. Phys.* **3**, 645–659 (2021).
8. Ishikawa, N., Sugita, M., Ishikawa, T., Koshihara, S.-Y. & Kaizu, Y. Lanthanide double-decker complexes functioning as magnets at the single-molecular level. *J. Am. Chem. Soc.* **125**, 8694–8695 (2003).
9. Woodruff, D. N., Winpenny, R. E. P. & Layfield, R. A. Lanthanide single-molecule magnets. *Chem. Rev.* **113**, 5110–5148 (2013).
10. Sessoli, R. & Powell, A. K. Strategies towards single molecule magnets based on lanthanide ions. *Coord. Chem. Rev.* **253**, 2328–2341 (2009).
11. Gregson, M. et al. A monometallic lanthanide bis(methanediide) single molecule magnet with a large energy barrier and complex spin relaxation behaviour. *Chem. Sci.* **7**, 155–165 (2016).
12. Liu, J. et al. A stable pentagonal bipyramidal Dy(III) single-ion magnet with a record magnetization reversal barrier over 1000 K. *J. Am. Chem. Soc.* **138**, 5441–5450 (2016).
13. Rinehart, J. D., Fang, M., Evans, W. J. & Long, J. R. Strong exchange and magnetic blocking in N23−-radical-bridged lanthanide complexes. *Nat. Chem.* **3**, 538–542 (2011).
14. Vitali, L. et al. Electronic structure of surface-supported bis(phthalocyaninato) terbium(III) single molecular magnets. *Nano Lett.* **8**, 3364–3368 (2008).
15. Komeda, T. et al. Observation and electric current control of a local spin in a single-molecule magnet. *Nat. Commun.* **2**, 217 (2011).
16. Thiele, S. et al. Electrically driven nuclear spin resonance in single-molecule magnets. *Science* **344**, 1135–1138 (2014).
17. Godfrin, C. et al. Electrical read-out of a single spin using an exchange-coupled quantum dot. *ACS Nano* **11**, 3984–3989 (2017).
18. Komijani, D. et al. Radical-lanthanide ferromagnetic interaction in a Tb^{III} bis-phthalocyaninato complex. *Phys. Rev. Mater.* **2**, 024405 (2018).
19. Trojan, K. L., Hatfield, W. E., Kepler, K. D. & Kirk, M. Strong exchange coupling in lanthanide bis-(phthalocyaninato) sandwich compounds. *J. Appl. Phys.* **69**, 6007 (1991).
20. Trojan, K. L., Kendall, J. L., Kepler, K. D. & Hatfield, W. E. Strong exchange coupling between the lanthanide ions and the phthalocyaninato ligand radical in bis(phthalocyaninato)lanthanide sandwich compounds. *Inorg. Chim. Acta* **795**, 198–200 (1992).
21. Fahrendorf, S. et al. Accessing 4f-states in single-molecule spintronics. *Nat. Commun.* **4**, 2425 (2013).
22. Warner, B. et al. Sub-molecular modulation of a 4f driven Kondo resonance by surface-induced asymmetry. *Nat. Commun.* **7**, 12785 (2016).
23. Frauhammer, T. et al. Indirect spin-readout of rare-earth-based single-molecule magnet with scanning tunneling microscopy. *Phys. Rev. Lett.* **127**, 123201 (2021).
24. Rizzini, A. et al. Coupling single molecule magnets to ferromagnetic substrates. *Phys. Rev. Lett.* **107**, 177205 (2011).
25. Marocchi, S. et al. Relay-like exchange mechanism through a spin radical between $TbPc_2$ molecules and graphene/Ni(111) substrates. *ACS Nano* **10**, 9353–9360 (2016).
26. Ara, F. et al. Control of the magnetic interaction between single-molecule magnet $TbPc_2$ and superconductor $NbSe_2$ surface by an intercalated Co atom. *Nano Lett.* **23**, 6900–6906 (2023).
27. Barhoumi, R. et al. Screening the 4*f*-electron spin of $TbPc_2$ single-molecule magnets on metal substrates by ligand channeling. *Nanoscale* **11**, 21167–21179 (2019).
28. Amokrane, A., Klyatskaya, S., Boero, M., Ruben, M. & Bucher, J.-P. Role of π-radicals in the spin connectivity of clusters and networks of Tb double-decker single molecule magnets. *ACS Nano* **11**, 10750–10760 (2017).
29. Fu, Y.-S. et al. Identifying charge states of molecules with spin-flip spectroscopy. *Phys. Rev. Lett.* **103**, 257202 (2009).
30. Swart, I., Sonnleitner, T. & Repp, J. Charge state control of molecules reveals modification of the tunneling barrier with intramolecular contrast. *Nano Lett.* **11**, 1580–1584 (2011).
31. Wu, S., Nazin, G., Chen, X., Qiu, X. & Ho, W. Control of relative tunneling rates in single molecule bipolar electron transport. *Phys. Rev. Lett.* **93**, 236802 (2004).
32. Nazin, G., Wu, S. & Ho, W. Tunneling rates in electron transport through double-barrier molecular junctions in a scanning tunneling microscope. *Proc. Natl. Acad. Sci. USA* **102**, 8832 (2005).
33. Mikaelian, G., Ogawa, N., Tu, X. & Ho, W. Atomic scale control of single molecule charging. *J. Chem. Phys.* **124**, 131101 (2006).
34. Fernández-Torrente, I., Kreikemeyer-Lorenzo, D., Stróżecka, A., Franke, K. J. & Pascual, J. I. Gating the charge state of single molecules by local electric fields. *Phys. Rev. Lett.* **108**, 036801 (2012).
35. Li, C. et al. Strong signature of electron-vibration coupling in molecules on Ag (111) triggered by tip-gated discharging. *Nat. Commun.* **14**, 5956 (2023).

36. Zhang, Y. et al. Detection and manipulation of charge states for double-decker $DyPc_2$ molecules on ultrathin CuO films. *ACS Nano* **12**, 2991–2997 (2018).
37. Kumar, D., Krull, C., Yin, Y., Medhekar, N. V. & Schiffrin, A. Electric field control of molecular charge state in a single-component 2D organic nanoarray. *ACS Nano* **13**, 11882–11890 (2019).
38. Yang, K. et al. Tuning the exchange bias on a single atom from 1 mT to 10 T. *Phys. Rev. Lett.* **122**, 227203 (2019).
39. Pederson, R., Wysocki, A. L., Mayhall, N. & Park, K. Multireference Ab initio studies of magnetic properties of terbium-based single-molecule magnets. *J. Phys. Chem. A* **123**, 6996–7006 (2019).
40. Huang, H., den Heuvel, W. V. & Soncini, A. Lanthanide-radical magnetic coupling in $[LnPc_2]^0$: competing exchange mechanisms captured via Ab initio multi-reference calculations. *Quantum Mater. Res.* **1**, e200003 (2020).
41. Shahed, S. M. F. et al. Observation of Yu–Shiba–Rusinov states and inelastic tunneling spectroscopy for intramolecule magnetic exchange interaction energy of terbium phthalocyanine (TbPc) species adsorbed on superconductor $NbSe_2$. *ACS Nano* **16**, 7651 (2022).
42. Heinrich, A. J., Gupta, J. A., Lutz, C. P. & Eigler, D. M. Single-atom spin-flip spectroscopy. *Science* **306**, 466–469 (2004).
43. Kawaguchi, R. et al. Spatially resolving electron spin resonance of π-radical in single-molecule magnet. *Nano Lett.* **23**, 213–219 (2022).
44. Schmidt, R. et al. Quantitative measurement of the magnetic exchange interaction across a vacuum gap. *Phys. Rev. Lett.* **106**, 257202 (2011).
45. Von Bergmann, K., Ternes, M., Loth, S., Lutz, C. P. & Heinrich, A. J. Spin polarization of the split Kondo state. *Phys. Rev. Lett.* **114**, 076601 (2015).
46. Branzoli, F. et al. Spin and charge dynamics in $[TbPc_2]^0$ and $[DyPc_2]^0$ single-molecule magnets. *Phys. Rev. B* **82**, 134401 (2010).
47. Zhang, Z.-M. et al. Atomic visualization and switching of ferroelectric order in β-In_2Se_3 films at the single layer limit. *Adv. Mater.* **34**, 2106951 (2021).
48. Nie, J.-H., Xie, T., Chen, G., Zhang, W.-H. & Fu, Y.-S. Moiré enhanced two-band superconductivity in a MnTe/$NbSe_2$ heterojunction. *Nano Lett.* **23**, 8370 (2023).
49. Kresse, G. & Furthmüller, J. Efficient iterative schemes for ab initio total-energy calculations using a plane-wave basis set. *Phys. Rev. B.* **54**, 11169 (1996).
50. Kresse, G. & Furthmüller, J. Efficiency of ab-initio total energy calculations for metals and semiconductors using a plane-wave basis set. *Comput. Mater. Sci.* **6**, 15 (1996).
51. Blöchl, P. E. Projector augmented-wave method. *Phys. Rev. B.* **50**, 17953 (1994).
52. Hamada, I. Van der Waals density functional made accurate. *Phys. Rev. B.* **89**, 121103(R) (2014).
53. Wang, V., Xu, N., Liu, J.-C., Tang, G. & Geng, W.-T. VASPKIT: a user-friendly interface facilitating high throughput computing and analysis using VASP code. *Comput. Phys. Commun.* **267**, 108033 (2021).
54. Liao, X. et al. Dataset: Spatially dependent f-π exchange interaction within a single-molecule magnet $TbPc_2$. *Zenodo*, https://doi.org/10.5281/zenodo.15644915 (2025).

Acknowledgements

The authors thank Emi Minamitani for fruitful discussions. This work is supported by the National Key Research and Development Program of China (Grants No. 2022YFA1402400), the National Science Foundation of China (Grants No. 12174131, 92265201, U20A6002, 92477137, 12322402, 12274206), the Natural Science Foundation of Hubei (2022CFB033) and Knowledge Innovation Program of Wuhan Basic Research (2023010201010056), Innovation Program for Quantum Science and Technology (Grant No. 2021ZD0302800), the National R&D Program of China (2022YFA1403601), the Natural Science Foundation of Jiangsu Province (No. BK20233001), and the Xiaomi foundation. M. R. and S. K. acknowledge the German Research Foundation (DFG) Collaborative Research Centre (CRC) 1573 "4*f* for Future".

Author contributions

X.L., X.T., L.Z.Y., and C.F.L. performed the experiments with the help of W.Z. and Y.S.F.; Y.C. did the theoretical modeling and simulations under the supervision of R.W.; R.J.S. carried out the DFT calculations; S.K. and M.R. synthesized the molecule; Y.S.F., W.Z., and X.L. analyzed the data and wrote the manuscript with comments from all authors. W.Z. and Y.S.F. supervised the project.

Competing interests

The authors declare no competing interests.

Additional information

Supplementary information The online version contains supplementary material available at https://doi.org/10.1038/s41467-025-61594-4.

Correspondence and requests for materials should be addressed to Wenhao Zhang or Ying-Shuang Fu.

Peer review information *Nature Communications* thanks Cyrus Hirjibehedin, Akseli Mansikkamäki, and the other anonymous reviewer(s) for their contribution to the peer review of this work. A peer review file is available.